PMSM Sensorless Control with Coordinate Rotation Digital Computer

Hung-Chi Chen (IEEE Member), Wei-Shun Huang, and Jhen-Yu Liao
Department of Electrical Engineering, National Chiao Tung University, HsinChu, Taiwan.
hcchen@cn.nctu.edu.tw

***Abstract*- Coordinate Rotation Digital Computer (CORDIC) is usually used to obtain the angle information without any multiply and division operations. The extended electromotive force (extended-EMF) in the literature shows that the angle error between the rotor reference frame and the assumed reference frame can be estimated from an arctangent function and a division. In this paper, the sensorless control for permanent-magnet synchronous motor (PMSM) is designed and implemented based on the CORDIC algorithm. Compared to the calculation of the arctangent function and division operation, CORDIC–based algorithm is able to save calculating time and memory resource. The provided simulation and experimental results also demonstrate the proposed CORDIC-based sensorless control.**

I. INTRODUCTION

The permanent-magnet synchronous motor (PMSM) is widely used in many applications, such as high-performance variable-speed drives. In order to control stator current and achieve a high-performance drive, the information of rotor position and speed are necessary. In most variable-speed drives, some type of shaft sensor such as optical encoder or resolver is connected to the rotor shaft. However, such sensor presents several disadvantages, such as drive cost, machine size, reliability, and noise immunity. Therefore, the sensorless control of a PMSM is desired, and various sensorless controls have been proposed.

The idea of extended electromotive force (extended-EMF) had been proposed and used in sensorless control [1-5] where a rotor reference frame is assumed. After some derivations, the angle difference between the assumed reference frame and the real rotor reference frame can be represented as arctangent value and division operator. However, it is not easy to implement arctangent function and division operator.

A simple algorithm based on the coordinate rotating digital computer (CORDIC) is a shift-and-add technique for computing a large class of mathematical functions [6-8]. In the applications, such as variable-speed control and robot, CORDIC is often used to obtain the angle information [9-10] without multiply function.

In this paper, CORDIC is used to calculate the angle difference by extended-EMF-based algorithms. Then, by forcing the angle difference to closed to zero, both rotor position and rotor speed are estimated by a simple PI-type regulator. The provided simulation and experimental results also demonstrate the proposed CORDIC-based sensorless control.

II. EXTENDED ELECTROMOTIVE FORCE (EXTENDED-EMF)

A. Rotor Reference Frame

In the PMSM control, machine variables are often transformed to d-q variables referred to the rotor reference frame where the direct axis (d-axis) is in the magnetic axis of the rotor permanent magnet and the quadrant axis (q-axis) is orthogonal to the d-axis. The voltage equations of PMSM in rotor reference frame can be represented as

$$\begin{bmatrix} V_d \\ V_q \end{bmatrix} = r\begin{bmatrix} i_d \\ i_q \end{bmatrix} + p\begin{bmatrix} L_d \cdot i_d \\ L_q \cdot i_q \end{bmatrix} + \omega_r \begin{bmatrix} -L_q \cdot i_q \\ L_d \cdot i_d \end{bmatrix} + \begin{bmatrix} 0 \\ E_0 \end{bmatrix} \quad (1)$$

where

L_d : the inductance along the d-axis path;
L_q : the inductance along the q-axis path;
V_d : the d-axis stator voltage;
V_q : the q-axis stator voltage;
i_d : the d-axis stator current;
i_q : the q-axis stator current;
r : the winding resistance per phase;
p : the time differentiation operator;
ω_r : the speed of the rotor and the rotor reference frame;
E_0 : the real electromotive force (EMF) in q-axis;

Rearranging the terms in (1), the voltage equations can be rewritten as

$$\begin{bmatrix} V_d \\ V_q \end{bmatrix} = r\begin{bmatrix} i_d \\ i_q \end{bmatrix} + pL_d\begin{bmatrix} i_d \\ i_q \end{bmatrix} + \omega_r L_q \begin{bmatrix} -i_q \\ i_d \end{bmatrix} + \begin{bmatrix} 0 \\ E_{0x} \end{bmatrix} \quad (2)$$

where the extended electromotive force (EEMF) E_{0x} is the sum of the real EMF term E_0 and some salient rerms

$$E_{0x} = E_0 + p(L_q - L_d)\cdot i_q + \omega_r (L_d - L_q)\cdot i_d \quad (3)$$

B. Assumed Reference Frame

In order to perform d-q transformation without position sensor, the assumed reference frame is also plotted in Fig. 1 where the angle signal $\Delta\theta$ is the difference between the angle θ_c of the assumed dc-qc reference frame and the angle θ_r of the d-q rotor reference frame.

$$\Delta\theta = \theta_c - \theta_r \quad (4)$$

978-1-4244-5226-2/10/$26.00 ©2010 IEEE

and

$$\frac{d\Delta\theta}{dt} = \frac{d\theta_c}{dt} - \frac{d\theta_r}{dt} = \omega_c - \omega_r \tag{5}$$

where ω_c is the rotation speed of the assumed dc-qc reference frame.

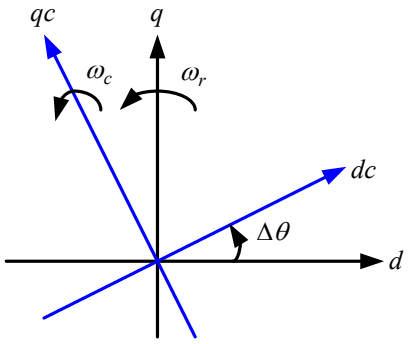

Fig. 1. Illustration of the assumed reference fame and the real rotor frame.

From Fig. 1, the relation between the dc-qc variables (F_{dc}, F_{qc}) and the d-q variables (F_d, F_q) can be represented as

$$\begin{bmatrix} F_d \\ F_q \end{bmatrix} = \begin{bmatrix} \cos\Delta\theta & -\sin\Delta\theta \\ \sin\Delta\theta & \cos\Delta\theta \end{bmatrix} \begin{bmatrix} F_{dc} \\ F_{qc} \end{bmatrix} = M \begin{bmatrix} F_{dc} \\ F_{qc} \end{bmatrix} \tag{6}$$

Applying (6) into (2) and rearranging the resulting terms yield

$$\begin{aligned} E_{0x} \cdot \begin{bmatrix} \sin\Delta\theta \\ \cos\Delta\theta \end{bmatrix} &= \begin{bmatrix} V_{dc} \\ V_{qc} \end{bmatrix} - r \begin{bmatrix} i_{dc} \\ i_{qc} \end{bmatrix} - pL_d \begin{bmatrix} i_{dc} \\ i_{qc} \end{bmatrix} \\ &\quad - \omega_c L_q \begin{bmatrix} -i_{qc} \\ i_{dc} \end{bmatrix} - \frac{d\Delta\theta}{dt}(L_d - L_q) \begin{bmatrix} -i_{qc} \\ i_{dc} \end{bmatrix} \end{aligned} \tag{7}$$

It follows that the angle difference $\Delta\theta$ can be obtained by

$$\Delta\theta = \tan^{-1}\left[\frac{V_x}{V_y}\right] \tag{8}$$

where

$$V_x = V_{dc} - (r + pL_d)\cdot i_{dc} + \left\{\omega_c L_q + (L_d - L_q)\frac{d\Delta\theta}{dt}\right\}\cdot i_{qc} \tag{9}$$

$$V_y = V_{qc} - (r + pL_d)\cdot i_{qc} - \left\{\omega_c L_q + (L_d - L_q)\frac{d\Delta\theta}{dt}\right\}\cdot i_{dc} \tag{10}$$

In non-salient PMSM, there is no difference between the inductances along rotor q-axis and d-axis ($L_q = L_d = L$), and thus, the angle difference $\Delta\theta$ in (8) can be simplified to

$$\Delta\theta = \tan^{-1}\left[\frac{V_{dc} - ri_{dc} + \omega_c L i_{qc}}{V_{qc} - ri_{qc} - \omega_c L i_{dc}}\right] \tag{11}$$

However, the derivative terms in (8) are near zero when the system is in the steady-state and thus, the angle difference $\Delta\theta$ in (8) can be simplified to

$$\Delta\theta = \tan^{-1}\left[\frac{V_{dc} - (r + pL_d)\cdot i_{dc} + \omega_c L_q i_{qc}}{V_{qc} - (r + pL_d)\cdot i_{qc} - \omega_c L_q i_{dc}}\right] \tag{12}$$

Consequently, from (4), the angle θ_r of rotor reference frame (i.e. rotor position) is also obtained by subtracting the angle difference $\Delta\theta$ from the angle θ_c of the assumed rotor reference frame.

Equation (8) is important, but implementing eq. (8) is hard because of the division operator and the arctangent function. Fortunately, CORDIC algorithm can be used to simplify the calculations .

III. CORDIC Algorithm

CORDIC is an algorithm used to compute trigonometric and hyperbolic functions easily using just bit shifts, lookup tables, and add operations, thus eliminating the need for multiplications.

The angle difference $\Delta\theta$ in (8) can be seen as the crossing angle of the initial vector (V_x^0, V_y^0) in the initial coordinate axis x_0 - y_0 as shown in Fig. 2. After rotating the coordinate axis with some given angles α_i, the unknown angle difference $\Delta\theta$ is available by summing all the given angles α_i after the final coordinate axis is aligning to the initial vector (V_x^0, V_y^0).

The new vector (V_x^i, V_y^i) in the new coordinate axis x_i - y_i is obtained by extending the vector length to $1/\cos\alpha_i$ and it can be represented as

$$\begin{aligned} \begin{bmatrix} V_x^i \\ V_y^i \end{bmatrix} &= \frac{1}{\cos\alpha_i} \begin{bmatrix} \cos\alpha_i & \sin\alpha_i \\ -\sin\alpha_i & \cos\alpha_i \end{bmatrix} \begin{bmatrix} V_x^{i-1} \\ V_y^{i-1} \end{bmatrix} \\ &= \begin{bmatrix} 1 & \tan\alpha_i \\ -\tan\alpha_i & 1 \end{bmatrix} \begin{bmatrix} V_x^{i-1} \\ V_y^{i-1} \end{bmatrix} \end{aligned} \tag{13}$$

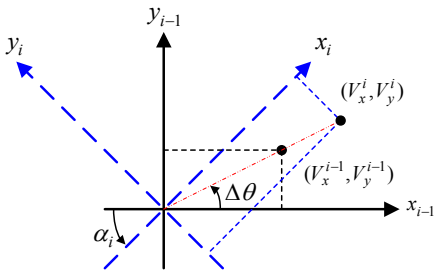

Fig. 2. Illustration of CORDIC.

If the given angles α_i are selected to be equal to $\tan^{-1}(2^{-n})$ with integer n, eq.(13) can be simplified to

$$\begin{bmatrix} V_x^i \\ V_y^i \end{bmatrix} = \begin{bmatrix} 1 & 2^{-n} \\ -2^{-n} & 1 \end{bmatrix} \begin{bmatrix} V_x^{i-1} \\ V_y^{i-1} \end{bmatrix} = \begin{bmatrix} V_x^{i-1} + 2^{-n} V_y^{i-1} \\ -2^{-n} V_x^{i-1} + V_y^{i-1} \end{bmatrix} \tag{14}$$

All the specific angles $\alpha_i = \tan^{-1}(2^{-n})$ are tabulated in Table I. The advantage of using such specific rotating angles is that the new vector (V_x^i, V_y^i) in the new coordinate axis x_i - y_i can be obtained by simple add operations and right-shift operations without any multiplying operations.

Table I Some specific rotating angles.

	$\tan(\alpha_i)$	α_i (degree)	α_i (rad)	$\frac{\tan(\alpha_i)}{\alpha_i}$	$\prod_{k=1}^{i}\frac{1}{\cos\alpha_k}$
1	±1	±45°	0.7854	1.273	1.4142
2	±1/2	±26.565°	0.4636	1.079	1.5811
3	±1/4	±14.036°	0.2450	1.020	1.6291
4	±1/8	±7.1250°	0.1243	1.006	1.6425
5	±1/16	±3.5763°	0.0624	1.002	1.6457
6	±1/32	±1.7899°	0.0312	1.001	1.6465

The CORDIC-based algorithms are:

(i) Decide the rotating direction

$$d_i = \begin{cases} +1, & when(V_x^{i-1}V_y^{i-1}) > 0 \\ -1 & when\ (V_x^{i-1}V_y^{i-1}) < 0 \end{cases} \tag{15}$$

(ii) Calculate the new vector

$$\begin{aligned} V_x^i &= V_x^{i-1} + d_i(2^{-i+1}V_y^{i-1}) \\ V_y^i &= -d_i(2^{-i+1}V_x^{i-1}) + V_y^{i-1} \end{aligned} \tag{16}$$

Finally, the unknown angle $\Delta\theta$ can be obtained by

$$\Delta\theta \approx \sum_{i=1}^{N} d_i\alpha_i \tag{17}$$

It is noted that after N recursive steps, the resulting variable V_y^i will approach to zero and the other one V_x^i will be closed to 5/3 times the length $\sqrt{(V_x^0)^2+(V_y^0)^2}$ of the original vector (V_x^0 , V_y^0).

Therefore, in order to avoid the overflow condition during each step, both input variables V_x and V_y should be attenuated with a gain $3/(5\sqrt{2}) \approx 0.4243$.

$$\begin{aligned} V_x^0 &= \frac{3}{5\sqrt{2}}V_x \\ V_y^0 &= \frac{3}{5\sqrt{2}}V_y \end{aligned} \tag{18}$$

IV. CORDIC-Based Sensorless Contorl

The proposed CORDIC-Based sensorless control is plotted in Fig. 3 where four PI-type controllers are included. The speed controller generates the q-axis current command I_{qc}^* from the speed command ω_r^* and the estimated speed ω_r . Then, two current controllers and the inverter yield the desired voltages to PMSM. The angle difference $\Delta\hat{\theta}$ is obtained from eq.(9-10) and eq.(15-17).

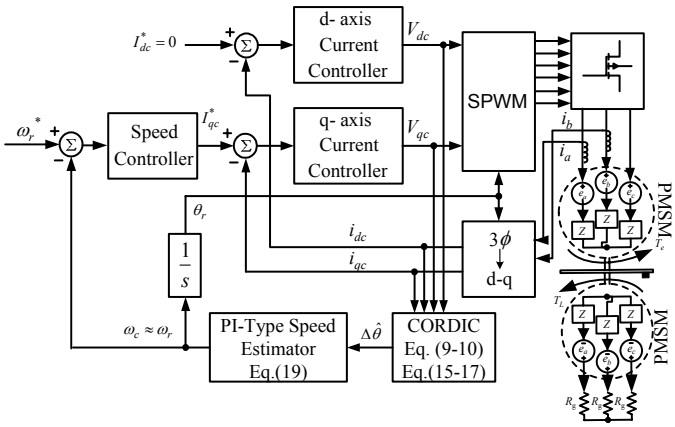

Fig. 3 CORDIC-Based sensorless control.

However, the positive angle difference $\Delta\hat{\theta}$ implies that the estimated rotor speed ω_c (i.e. the speed of the assumed reference frame) is larger than the real rotor speed ω_r . Therefore, the estimated rotor speed ω_c should be decreased to reduce the positive angle difference $\Delta\hat{\theta}$.

On the other hand, the negative angle difference $\Delta\hat{\theta}$ means that the estimated rotor speed ω_c is smaller than the real rotor speed ω_r , and thus, the estimated rotor speed ω_c should be increased. Once the calculated $\Delta\hat{\theta}$ is near zero, no change of the estimated rotor speed ω_c is needed.

Consequently, these principles can be achieved by a simple PI controller,

$$\omega_c = -\frac{sK_p + K_i}{s}\Delta\hat{\theta} \tag{19}$$

When PMSM is standstill, the back-EMFs are zero and the proposed sensorless control needs starting strategy. The proposed starting strategy divided into constant current mode (CCM) and constant speed mode (CSM) is plotted in Fig. 4.

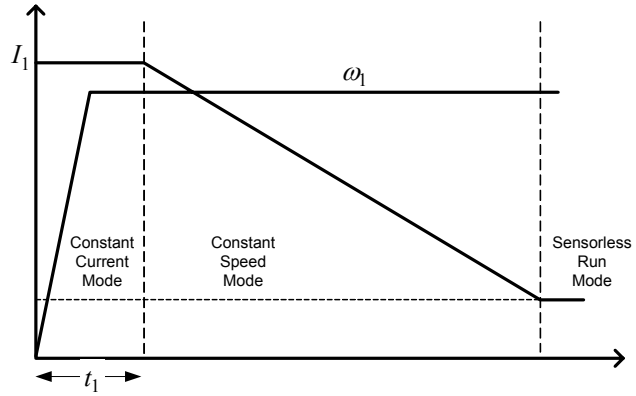

Fig. 4 Starting modes.

In CCM, the q-axis current command is given to $I_{qc}^* = I_1$ with zero d-axis current command $I_{dc}^* = 0$. The speed ω_c of the assumed reference frame initially increases from zero with a fixed rate and then, keeps to a constant ω_1 .

After a given time t_1 , the operating mode changes from CCM to CSM. In CSM, the q-axis current command I_{qc}^* decreases linearly, and the speed ω_c of the assumed reference frame keeps constant. At the same time, the angle

difference $\Delta\hat{\theta}$ is calculated and checked if the angle difference $\Delta\hat{\theta}$ is near zero. Once the angle difference $\Delta\hat{\theta}$ is between $-3°$ to $+3°$, the operation mode will change from CSM to sensorless run mode (SRM).

V. Simulation Results

In this section, some simulation results are provided to demonstrate the proposed CORDIC-based Sensorless control. The used simulation software is PSIM and the parameters of PMSM are tabulated in Table II.

Table II. Simulation parameters

Stator resistance	2.2Ω
Stator inductance	$Lq = 4.58mH$ $Ld = 3.61mH$
Voltage constant (Line-to-Line)	$75V_{rms} / krpm$
Pole number	*4* pole
Motor inertia	$0.000161\, kgm^2$

The simulated waveforms during the starting period are plotted in Fig. 6. Initially, PMSM is forced to rotate by the attraction force between the stator magnetic field and the rotor PM. Thus, the operation of PMSM in CCM can be seen as a synchronous motor with large rotor angle (near to $90°$).

With the decrease of PMSM current amplitudes in CSM, the rotor angle of PMSM also decreases to generate constant torque under fixed speed. Thus, the calculated angle difference $\Delta\hat{\theta}$ decrease, and the yield motor current i_a is in phase with the back-EMF e_a gradually.

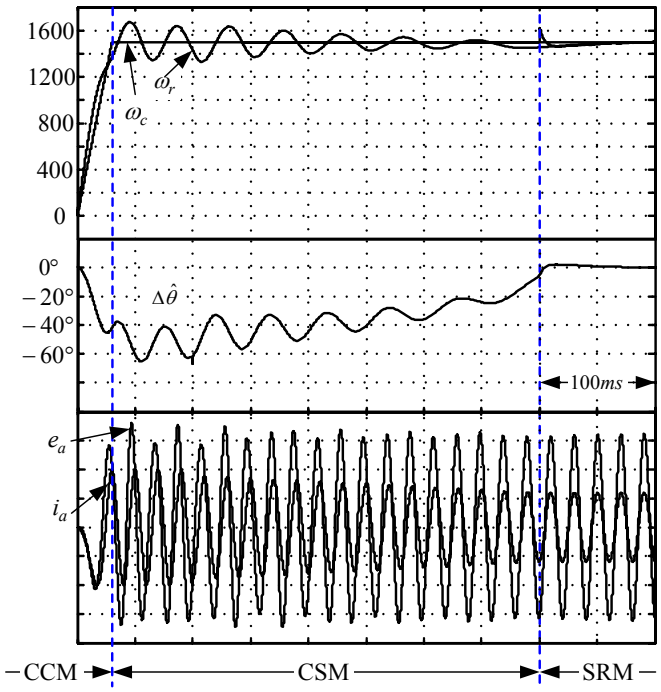

Fig. 6. Simulated waveforms during the starting period.

After the calculated angle difference $\Delta\hat{\theta}$ is smaller than $3°$, the operation mode changes from CSM to SRM. The simulated waveforms with speed 2000rpm are plotted in Fig. 7.

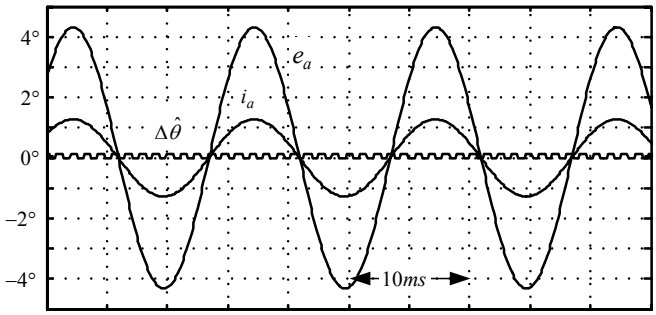

Fig. 7. Simulated waveforms at 2000rpm.

VI. Experimental Results

Two identified PMSM are coupled to each other to become the M-G set and the three-phase Y-connected resistors are connected to one of the two PMSM (i.e. generator). The Encoder position signals are also feedback to the control system for comparison.

The CORDDIC-based sensorless control in Fig. 3 had been implemented in DSP TMS320F2812 and some experimental results are provided in this section. The PWM frequency is 6.67kHz and the experimental waveforms in 2000rpm and 3000rpm are plotted in Fig. 8 and Fig. 9, respectively.

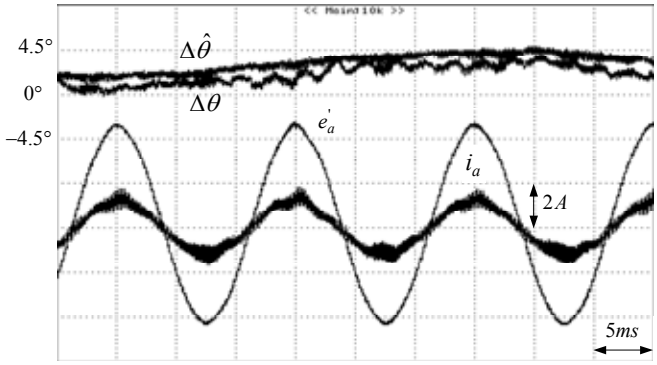

Fig. 8. Experimental waveforms at 2000rpm.

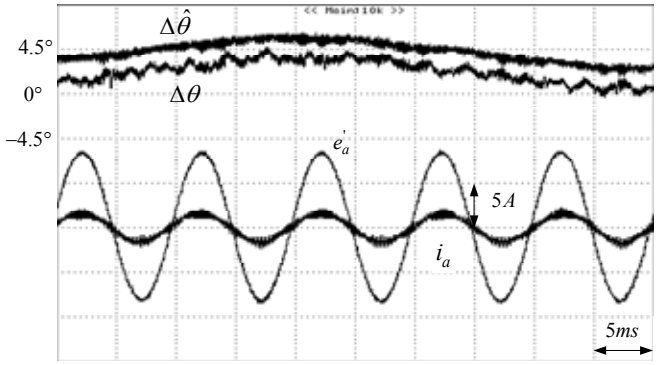

Fig. 9. Experimental waveforms at 2000rpm.

The real angle difference $\Delta\theta$ is obtained from the real rotor position for comparison, and the estimated angle difference $\Delta\hat{\theta}$ is calculated from (17). It is noted that the estimated angle difference $\Delta\hat{\theta}$ is very closed to the real angle difference $\Delta\theta$. On the other hand, the yielded motor current i_a is sinusoidal and in phase with the pseudo back-EMF waveform $e_a^{'}$ which is obtained from the real rotor position.

The waveforms corresponding to the speed change are plotted in Fig. 10 where the speed command ω_r^* is changed from 1000rpm to 3000rpm, and then, returned to 1000rpm with fixed rising and falling rates. Larger estimated angle difference $\Delta\hat{\theta}$ can be found when the motor speed is changing. However, the speed control is stable. Thus, the provided experimental waveforms demonstrate the proposed CORDIC-based sensorless control.

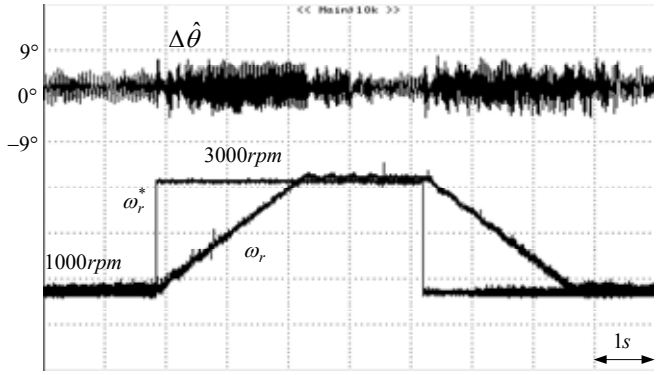

Fig. 10. Experimental waveforms with the change of the speed command.

VII. CONCLUSIONS

In this paper, a CORDIC-based sensorless control is proposed and implemented. The results show that the economical CORDIC-based algorithms are able to obtain acceptable value. However, the parameter accuracy has a great effect on the control performance. Robust control performance under parameter uncertainty is the future work.

REFERENCES

[1] S. Ichikawa, M. Tomita, S. Doki, and S. Okuma, "Sensorless control of permanent-magnet synchronous motors using online parameter identification based on system identification theory," *IEEE Trans. Ind. Electron.*, vol.53, no. 2, pp. 363–372, Apr. 2006.

[2] S. Ichikawa, M. Tomita, S. Doki, and S. Okuma, "Sensorless control of synchronous reluctance motors based on extended EMF models considering magnetic saturation with online parameter identification," *IEEE Trans. Industry Applications.*, vol. 42, no. 5, pp. 1264–1274, Sep. 2006.

[3] H. Kim, M. C. Harke and R. D. Lorenz, "Sensorless control of interior permanent-magnet machine drives with zero-phase lag position estimation," *IEEE Trans. Industry Applications.*, vol. 39, no. 6, pp. 1726–1733, Nov. 2003.

[4] S. Morimoto, K. Kawamoto, M. Sanada and Y. Takeda, "Sensorless control strategy for salient-pole PMSM based on extended EMF in rotating reference frame," *IEEE Trans. Industry Applications.*, vol. 38, no. 4, pp. 1054–1061, July 2002.

[5] S. Morimoto, K. Kawamoto, M. Sanada and Y. Takeda, "Mechanical sensorless drives of IPMSM with online parameter identification," *IEEE Trans. Industry Applications.*, vol. 42, no. 5, pp. 1241–1248, Sep., 2006.

[6] K. Kota and J. R. Cavallaro, "Numerical Accuracy and Hardware Tradeoff for CORDIC Arithmetic for Special-Purpose Processors," *IEEE Trans. Computers*, vol. 42, no. 7, pp. 769–779, July, 1993.

[7] N. Takagi, T. Asada and S. Yajima, "Redundant CORDIC Methods with a constant Scale Factor for Sine and Cosine Computation", *IEEE Trans. Computers*, vol. 40, no. 9, pp. 989-995, Sep., 1991.

[8] S. F. Hsiao and C. Y. Lau, "Design of a Unified Arithmetic Processor based on Redundant Constant-factor CORDIC with Merged Scaling Operation", *IEE Proc. Comput. Digit. Tech.,* vol. 147, no. 4, pp. 297-303, July, 2000.

[9] D. H. Kitabjian and P. R. Chitrapu, "The Suboptimality of Angle Coding in the CORDIC Algorithm", 1992.

[10] L. Vachhani, K. Sridharan and P. K. Meher, "Efficient FPGA Realization of CORDIC with Application to Robotic Exploration", *IEEE Trans. Industrial Electronics*, vol. 56, no. 12, pp. 4915–4930, Dec. 2009.